Applicability of Nosé isothermal reversible dynamics

Francesco D. Di Tolla* and Marco Ronchetti
Dipartimento di Fisica, Università degli Studi di Trento, 38050 Povo (TN), Italy
(Received 2 March 1993)

In this work we characterize the conditions under which the Nosé approach to isothermal molecular dynamics applied to a nontrivial system yields time averages that are equivalent to canonical phase averages, i.e., we determine when the (extended) system verifies the quasiergodic property. Our results show that the dynamics can be *tuned* to produce a resonance between the characteristic frequencies of the heat bath and those of the thermalized system by choosing a proper value for the inertia of the heat bath.

PACS number(s): 05.20.Gg, 02.60.−x, 02.70.−c

I. INTRODUCTION

Molecular dynamics (MD) is a well-known technique for simulating time evolution of a classical many-body system. It consists basically in the numerical solution of the Newton differential equations of motion. This technique, first introduced by Rahman [1] in 1964, has been widely applied to the simulation of condensed matter. It is well described in books [2,3] and seminal papers in which this technique was used have been reprinted in special volumes [4]. In the most simple and common formulation of MD the particles are contained in a fixed size and fixed shape cell which is periodically repeated in space so as to simulate an infinite system. Cell volume, number of particles, total energy, and total linear momentum are conserved throughout the simulation. Under these conditions, the time averages are considered to be taken in the *microcanonical* or (N,V,E) ensemble (although also the internal stresses are conserved, due to rigidity of the simulation cell).

Often, however, other statistical ensembles are more interesting, since in the simulation of a real situation other thermodynamic functions (such as temperature, pressure, chemical potential) must be kept constant. In some way these functions are conjugated with respect to those conserved in the microcanonical ensemble. In fact to conserve temperature we should allow the energy to fluctuate in time and therefore the corresponding ensemble is the *canonical* one, or (N,V,T). Similarly, to conserve at the same time temperature and pressure, the energy and the volume should evolve dynamically, as in the *isobaric-isothermal* or (N,p,T) ensemble. If instead we want to conserve temperature and chemical potential μ, the energy and the number of particles should vary in time and the appropriate statistical ensemble is the *grand canonical* or (μ,V,T). Other combinations of conserved functions are possible but they describe situations of lesser physical interest.

Many modifications of the basic Verlet [5] algorithm were proposed to simulate different statistical ensembles. In particular, many authors derived algorithms for simulating systems at constant temperature: among these the rescaling algorithm [6], the Gauss-constrained dynamics [7], or the stochastic collision method [8]. These formulations presented various problems such as discontinuity in the trajectories, noncausal dynamics, or bad reproduction of thermodynamic fluctuations, if compared to the expected values of a canonical ensemble. Such limitations were overcome by a Hamiltonian approach first proposed by Nosé [9] in 1984 and later reformulated by Hoover [10]. Nosé dynamics has been applied to many probes, but it is still unknown whether it produces a true canonical distribution when applied to systems which are extended in size. Nosé dynamics is now very important because it is used in the *ab initio* molecular dynamics (Car-Parrinello) to keep the electrons in their ground state.

In the present work we study the parameters which appear in the formulation so as to verify under which conditions the system is in fact canonical. We therefore determine when the quasiergodic property is verified by studying the characteristic frequencies of the system, the energy distribution, power spectrum, and time correlations.

The paper is organized as follows: in Sec. II we introduce the formalisms proposed by Nosé [9] and Hoover [10] and we supply an attempt of interpretation of those schemes. In Sec. III we try to verify *a posteriori* the ergodicity of the system by comparing the simulation results with the theoretical estimations made in the canonical ensemble. In Sec. IV we draw our conclusions.

II. SIMULATION IN THE CANONICAL ENSEMBLE

A. Nosé isothermal dynamics and canonical ensemble

In 1984 Nosé proposed [9] a Hamiltonian approach to perform an isothermal dynamics (i.e., a simulation in which the temperature is held at a given value). In this case the author showed that under proper conditions the N-particle system has exactly a canonical distribution in phase space (in general, an isothermal dynamics will not necessarily produce a canonical distribution, and conversely there is no unique dynamics associated to a canonical distribution).

In his formulation, Nosé extended the usual $6N$-dimensional phase space $(\mathbf{x}_i,\mathbf{p}_i)$ of the *real system* by adding one extra variable and its conjugate momentum. The idea of extending the system was originally presented

by Andersen for the simulation in an isobaric-isoenthalpic ensemble [8]. According to Nosé, the *extended systems* phase space is described by coordinates $(\mathbf{q}_i, \pi_i, s, \pi_s)$, where s is the extra degree of freedom which should describe a virtual heat bath and π_s is the relative conjugate momentum. $\mathbf{q}_i$, π_i are related to the original coordinates by the relations

$$\begin{aligned} \mathbf{x}_i &= \mathbf{q}_i \ , \\ \mathbf{p}_i &= \frac{\pi_i}{\mathbf{s}} \ . \end{aligned} \tag{1}$$

The extended systems Hamiltonian is postulated to be as follows:

$$\begin{aligned} H_N(\mathbf{x}_i, \pi_i, s, \pi_s) &= \sum_i \frac{\pi_i^2}{2m_i s^2} + \phi(\{\mathbf{x}_i\}) + \frac{\pi_s^2}{2Q} + g k_B T_0 \ln(s) \\ &= H_0\left[\frac{\pi_i}{s}, \mathbf{q}_i\right] + \frac{\pi_s^2}{2Q} + g k_B T_0 \ln(s) \ , \end{aligned} \tag{2}$$

where Q is a parameter which controls the inertia to the evolution of s, g is connected to the number of degrees of freedom of the system, T_0 is the bath temperature, and k_B is the Boltzmann constant.

The evolution is calculated with respect of a virtual time τ defined as

$$d\tau = s\, dt \tag{3}$$

and the Hamilton equations of motion are

$$\frac{d\mathbf{x}_i}{d\tau} = \frac{\pi_i}{m_i s^2} \ , \tag{4a}$$

$$\frac{d\pi_i}{d\tau} = -\frac{\partial \phi(\{\mathbf{x}_i\})}{\partial \mathbf{x}_i} = -\frac{\partial \phi(\{\mathbf{q}_i\})}{\partial \mathbf{q}_i} \ , \tag{4b}$$

$$\frac{ds}{d\tau} = \frac{\pi_s}{Q} \ , \tag{4c}$$

$$\frac{d\pi_s}{d\tau} = \frac{1}{s}\left[\sum_i \frac{\pi_i^2}{m_i s^2} - g k_B T_0\right] \ . \tag{4d}$$

Nosé showed that by choosing $g = 3N + 1$, the microcanonical ensemble average of any function $A(\pi_i/s, \mathbf{q}_i)$ taken over the extended system is equivalent to a canonical average for the same function in the real system. Moreover, if the extended system is quasiergodic one has the relation

$$\begin{aligned} \lim_{\tau_0 \to \infty} \frac{1}{\tau_0} \int_0^{\tau_0} A(\pi_i/s, \mathbf{x}_i)\, d\tau &= \langle A(\pi_i/s, \mathbf{x}_i) \rangle_{\mu c} \\ &= \langle A(\mathbf{p}_i, \mathbf{q}_i) \rangle_c \ , \end{aligned} \tag{5}$$

i.e., the time average on a long enough trajectory from a microcanonical simulation in the extended system gives an estimation of the canonical phase-space average in the real system.

At the same time Eqs. (4c) and (4d) can be combined to give

$$\frac{d^2 s}{d\tau^2} = \frac{1}{Qs}\left[\sum_i m_i s^2 \left[\frac{dx_i}{d\tau}\right]^2 - g k_B T_0\right] \ , \tag{6}$$

which fixes the (thermodynamic) temperature at the desired value.

Since when it was formulated, it was clear that the quasiergodic hypothesis could not be studied analytically, except for trivial systems. For instance, we know that a system is quasiergodic if and only if the constant-energy surface is a *metrically indecomposable* manifold [11]. However, as Kinchin showed, this does not happen when we have other integrals whose value is fixed from the procedure of preparation of the sample [12]. Hence we should deal with a *weak* quasiergodic hypothesis, related to the indecomposability *in an extended sense* of the submanifold characterized by the energy and all other *controllable* integrals (or *normal* phase functions), like the three components of the linear momentum.

For complex systems the best we can do is to verify *a posteriori* whether the observed behavior is canonical or not:

> . . . when we are not able to submit really convincing arguments in favor of replacing the time averages by the phase averages, it is preferable, and also simpler, to attempt as the "ergodic hypothesis" the very possibility of such a replacement, and then to judge the theory constructed on the basis of this hypothesis, by its practical success or failure [13].

To test the hypothesis we have to compare the theoretical predictions with the observed behavior: for instance, we can predict the distribution of the total energy and the momenta of various order of the distribution of the kinetic energy.

Alternatively we can verify whether the system shows the so-called *mixing property,* i.e., if every correlation between dynamical variables vanishes for large time lags. It has been demonstrated that the mixing property implies quasiergodicity although the converse is not true [14].

Analytically we say that a system shows the mixing property when each pair of measurable sets A and B of the ergodic surface does satisfy the following relation:

$$\lim_{t \to \infty} \mu[\varphi_t(A) \cap B] = \mu(A)\mu(B) \ ,$$

where $\varphi_t(A)$ is the set composed by the points initially belonging to A, propagated for t seconds with the equations of motion.

B. Real time Nosé dynamics and Nosé-Hoover dynamics

As we have seen, the extended system formulation implies a mapping of the *real system* time into a virtual time τ through the variable s. Since the time step used in the calculation is constant in virtual time, the real system trajectories are described with a nonuniform (real) time step. Nosé showed [15] that the extended system approach can be reformulated so as to work in real time. A similar reformulation has been proposed by Hoover [10]. We find Hoover's formulation more convenient, since it requires

no redefinition of π_s and the couple (s,π_s) is replaced by a single variable ζ defined by

$$\zeta=\frac{d\ln(s)}{dt}=\frac{\dot{s}}{s}=\frac{P_s}{Q} .$$

In this case we need only a closed set of three equations:

$$\dot{\mathbf{q}}_i=\frac{p_i}{m_i} , \tag{7a}$$

$$\dot{\mathbf{p}}_i=-\frac{\partial\phi(\mathbf{q}_i)}{\partial\mathbf{q}_i}-\zeta\mathbf{p}_i , \tag{7b}$$

$$\dot{\zeta}=\frac{2}{Q}\left[\sum_i\frac{\mathbf{p}_i^2}{2m_i}-\frac{g}{2}k_BT_0\right] . \tag{7c}$$

This scheme is non-Hamiltonian and during the time evolution a pseudoenergy is conserved

$$\varepsilon=\sum_i\frac{\mathbf{p}_i^2}{2m_i}+\phi(\mathbf{q}_i)+\frac{Q\zeta^2}{2}+gk_BT_0\int_0^t d\tau\,\zeta(\tau) ,$$

where $g=3N$ is the only value which gives the canonical distribution.

This approach is similar, but not strictly equivalent, to the former. If we require the trajectories in the two schemes to have the same embedding in phase space as geometrical loci of points, we have to use the same value for g, in both sets of equations. However, due to the different definition of the time in the two frames, the same point in phase space would then be passed through at different speed by the representative points of the two systems. Therefore the points visited by the sample trajectory (generated by the same initial condition in both frames) would receive different weights, and in general the time averages along the two sample trajectories would be different and would not yield the same phase average. To actually get equivalent results with different time definition (weighting), we need different trajectories, hence different equations, or different values for g.

This last fact we made clear by the work of Jellinek [16,17], who also introduced a full class of different Hamiltonians in proper extended spaces, which should produce a canonical distribution in the related real space, under ergodicity in a weighted-microcanonical sense in the extended system. We are not aware of any practical application of this methods in literature. The original work presents some conclusions about the application of this generalized approach without data to support them. Cagin [18] tried to apply at the same time a scaling to the momenta and to the coordinates as suggested by Jellinek, but in this case the coupling controlled at the same time the temperature and the pressure in a way that is not yet well understood.

C. Interpretation of the coupling scheme

Hoover's reformulation makes clearer the meaning of the coupling to the thermal bath by showing that it is equivalent to the introduction of a friction term in the equations of motion for the π_i (7b). This is similar to what happens in the constrained algorithm [7] (Gauss thermostat), in which the equation of motion for the coordinates and momenta are the same as in (7a) and (7b), but ζ is a Lagrange multiplier, rather than a variable of the system. In this case the instantaneous value of ζ does not evolve following equation (7c), but is determined by the Gauss least-constrained principle, in order to hold the kinetic energy fixed. At each time step we can compute it with the relation

$$\zeta_G=-\frac{\sum_i\mathbf{F}_i\frac{\mathbf{p}_i}{m_i}}{\sum_i\frac{\mathbf{p}_i^2}{m_i}} .$$

Another general way to introduce the Nosé-Hoover thermostat is to suggest Eqs. (7a) and (7b) as a generalized Newton dynamics and then to require that the Liouville equation, written in the general form

$$\frac{\partial f}{\partial t}+\frac{\partial(f\dot{\Gamma})}{\partial\Gamma}=0 ,$$

have a stable solution for the density $f=f(\mathbf{p},\mathbf{q},\zeta)$ in phase space of the form

$$f(p,q,\zeta)\propto g(\zeta)e^{-H_0(p,q)/k_BT} , \tag{8}$$

i.e., equivalent to the canonical phase-space distribution.

In (2) H_0 is the Hamiltonian of the real system

$$H_0=\sum_i\frac{\mathbf{p}_i^2}{2m_i}+\phi(\{\mathbf{q}_i\})$$

and $g(\zeta)$ should satisfy

$$\int g(\zeta)d\zeta<\infty$$

to produce a finite partition function, and $g(\zeta)>0$ to respect the positive definiteness of the density itself. In Hoover's frame,

$$g(\zeta)=e^{-\zeta^2/k_BT} .$$

The constraint $\partial\dot{\zeta}/\partial\zeta=0$ determines uniquely the form of the equation for the evolution for the ζ itself (7c).

Bulgac and Kusnezov showed [19–21] that this method could be generalized adding a general kind of friction term to both equations for $\mathbf{q}_i$ and π_i,

$$\dot{\mathbf{q}}_i=\frac{\mathbf{p}_i}{m_i}-h_2(\xi)\mathbf{F}_i(\mathbf{p}_i,\mathbf{q}_i) , \tag{9a}$$

$$\dot{\mathbf{p}}_i=-\frac{\partial\phi(\mathbf{q}_i)}{\partial\mathbf{q}_i}-h_1(\zeta)\mathbf{G}_i(\mathbf{p}_i,\mathbf{q}_i) , \tag{9b}$$

and requiring to have a solution to Eq. (8) of the form

$$f(p,q,\zeta,\xi)=(1/N)\exp\{-[H_0+g_1(\zeta)/\alpha+g_2(\xi)/\beta]k_BT\},$$

where one has the freedom to choose the constants α and β and the functions g_i.

As before one adds the constraints $\partial\dot{\zeta}/\partial\zeta=0$ and $\partial\dot{\xi}/\partial\xi=0$ and finds an expression for the functions h_i,

$$h_1(\zeta)=\frac{\delta g_1(\zeta)}{\delta\zeta} , \quad h_2(\xi)=\frac{\delta g_2(\xi)}{\partial\xi} ,$$

and the following equations of motion for the extension variables:

$$\dot{\zeta}=\alpha\left\{\frac{\partial H}{\partial \mathbf{p}_i}\mathbf{G}_i-k_BT\frac{\partial \mathbf{G}_i}{\partial \mathbf{p}_i}\right\}, \quad \dot{\xi}=\beta\left\{\frac{\partial H}{\partial \mathbf{q}_i}\mathbf{F}_i-k_BT\frac{\partial \mathbf{F}_i}{\partial \mathbf{p}_i}\right\}.$$

Moreover we stress that Nosé-Hoover and Bulgac-Kusnezov dynamics have the general property that at equilibrium the phase averages of the functions h_i are vanishing and hence the friction terms do not affect the Hamiltonian structure of the equations on average [10,15,20,21].

This method has been compared to Nosé and Nosé-Hoover schemes to verify if a single oscillator coupled to a thermostat behaves as predicted.

It has been found [22] that for particular initial conditions and Q values the Nosé dynamic could be nonergodic, probably because it is not enough chaotic.

Nosé-Hoover equations produced trajectories with a higher degree of chaoticity; the proper choice of the parameters and of the form of the functions involving the Bulgac-Kusnezov approach had the highest degree of mixing and the best reproduction of the expected distribution of the observables studied [20,21].

It is important to underline that from these negative results we cannot argue anything about the validity of the scheme applied to systems extended in size.

There are only two results concerning extensions to a small number of oscillators and they furnished opposite results.

Posch [22] was not able to find critical initial condition for a system of two *soft spheres* coupled mutually and to a virtual bath, i.e., the observed behavior was always canonical.

Conversely, Nosé found [23] a critical behavior for a system of a few free oscillators coupled only through a common heat bath with Hoover's equations of motion; the results were strongly dependent on the mutual ratios of the characteristic frequencies of the oscillators. Similar problems should be present in the simulation of any system in the solid phase because of the possibility of approximating any such system with a set of free oscillators, for low enough temperature.

III. SIMULATION IN THE SOLID STATE

A. Nosé dynamics in the solid state

Nosé dynamics has been applied to many probes, but it has never been demonstrated whether it samples properly the canonical phase space when applied to a system extended in size.

The correct value for the temperature is easily reproduced in the simulations, but a few numerical experiments from Nosé showed that it is not easy to reproduce the "right" amount of fluctuations for the thermodynamic state functions. (Nosé worked with a liquid [8] and also studied the diffusion coefficient.)

With a simple theoretical argument Cho and Joannopoulos showed [24,25] that hard-sphere systems cannot produce the expected behavior, because that kind of potential does not guaranty the equipartition of the energy among the degrees of freedom.

In this work we applied Nosé equations to a system of 256 Lennard-Jones atoms in periodic boundary conditions in the solid state (most of the cases $T_0=0.4$, $\rho=0.973$ in Lennard-Jones units or $T_0=50$ K, $\rho=1.61$ g/cm^3 for argon), and we studied the influence of the value of the thermal inertia Q, varying it over more than five orders of magnitude.

Nosé suggested [26] that the Q variable should be neither "too big" nor "too small." He showed that a too large value of Q slows down the evolution of the s variable and produces only a slow feedback of the temperature. Hoover [3] argued that a too small value of Q will produce the wrong amount of fluctuations for the kinetic energy.

In Hoover's frame we can rewrite Eq. (7c) in the form

$$\dot{\zeta}=2\left[\frac{\pi}{\tau}\right]^2\left[\frac{K}{K_0}-1\right],$$

where K is the kinetic energy of the system, K_0 is connected to T_0 in the obvious way,

$$K_0=\frac{g}{2}k_BT_0,$$

and the constant τ,

$$\tau=2\pi\sqrt{Q/2gk_BT_0},$$

has the dimensions of a time, and fixes the time scale of the thermostat's response to the departure of the kinetic energy from its mean value.

If τ (or Q) goes to zero we will produce an instantaneous control of the temperature and a behavior identical to the one produced by a Gauss thermostat: kinetic-energy fluctuations are completely suppressed.

Before tracing the differences in the results obtained with different Q values we recall that Eq. (6) can be linearized if $\langle s\rangle$ is near to 1, expanding s around its mean value and defining δs as

$$\delta s=s-\langle s\rangle.$$

δs obeys to the simple equation

$$\frac{d^2}{dt^2}(\delta s)+\omega^2\delta s=0,$$

i.e., the s variable should present a periodic behavior at a well-defined frequency, which has been nicely estimated by Nosé [26] in two limiting cases: for very small values of Q

$$\omega_1=\sqrt{2gk_BT_0/Q} \tag{10a}$$

and for large values of Q

$$\omega_2=\sqrt{g^2k_B^2T_0/QC_V}=\omega_1\sqrt{gk_B/2C_V}, \tag{10b}$$

where C_V is the heat capacity at constant volume.

B. Power spectral density of s

We investigated the influence of the Q parameter which controls the strength of the coupling between the bath variable s and the atoms. Q was varied over several

orders of magnitude: from 0.01 to 1000. We use Lennard-Jones units for Q [to transform in the units used by Nosé in his works (kJ $(ps)^2$ mol^{-1}) one has to multiply by 4.744 our values]. All our samples contained 256 particles interacting through a Lennard-Jones potential with parameters suited for argon ($\sigma = 3.446$ Å and $\varepsilon = 125$ K). We used a time step of 0.002 34, i.e., 5×10^{-15} s. For all cases we started from an fcc lattice in periodic boundary conditions an set the thermostat temperature at $0.4\varepsilon = 50$ K (melting point is at 84 K). This brings the first issue, which concerns the reaching of an equilibrium state. In fact, Nosé equations describe a thermostated system at equilibrium, but it is not *a priori* guaranteed that a system will reach the equilibrium itself.

In a typical constant-energy simulation, one knows the average position of the atoms (the crystalline lattice) and the distribution of the velocities (a Maxwellian). One therefore starts from the ideal lattice and introduces random displacements: the resulting velocities are then normalized so as to reach the desired temperature. In a short time the system reaches an equilibrium state. The system equilibration, which consists in throwing away the first few thousand steps, guarantees in practice that measured observables (such as pair distribution functions, velocity autocorrelations, etc.) do not depend from the initial preparation but only on the thermodynamic state of the system.

In a constant-temperature simulation, one should make sure that the extended system (which includes the s variable and its conjugate momentum) reaches equilibrium. A procedure like the one employed in the constant-energy case introduces, however, spurious temperature oscillations that die out rather slowly. We found that the most effective way to prepare a sample is to equilibrate the system in the microcanonical ensemble at an average temperature roughly equal to the desired one, and then to switch the Nosé thermostat on. This can be seen in some of the figures shown later (Figs. 1, 4, and 9) where we have performed an equilibration of 500 time steps of simulation in the (N,V,E) ensemble before "applying" the thermostat. A more sophisticated method for damping the temperature oscillation caused by the initial choice is based on a chain of Nosé thermostats, as recently suggested by Martyna, Klein, and Tuckerman [27].

After reaching equilibrium, we started monitoring the time evolution of the relevant quantities [the s variable and the instantaneous temperature, i.e., the kinetic energy (KE) of the atoms]. In Fig. 1 we show the time evolution of s for two values of Q. At $Q = 100$ [Fig. 1(a)] s oscillates rather regularly: there seems to be a well-defined frequency, and the oscillation amplitude does not vary much, at least on the time scale we choose for the simulation (17 000 time steps). At $Q = 0.1$ [Fig. 1(b)] the behavior is quite different: the frequency is much higher, which one would expect since Q plays the role of an inertia in the s dynamics. In addition, the amplitude of the oscillations varies strongly in time.

It is interesting to analyze the frequency spectrum of these time series. We calculated the power spectral density (PSD) of $s(t)$ either by computing the squared modulus of the Fourier transform of the signal or using

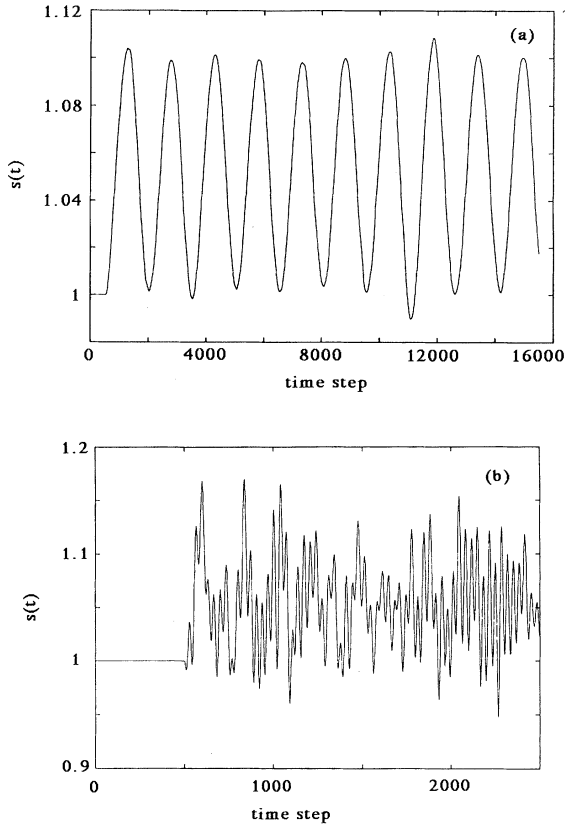

FIG. 1. Time evolution of s for $Q = 100$ (a), $Q = 0.1$ (b). The initial 500 steps were performed at constant energy to equilibrate the system.

parametric methods called autoregressive moving average methods (ARMA modeling).

The first algorithm is based on the fast Fourier transform (FFT), a well-known numerical tool for the estimation of Fourier transform of discrete time series. The second is less common and is used in general signal processing problems [28]. It is essentially based on the idea that the discrete-time signal under study is the output of a causal linear filter whose input is a white noise of indeterminate variance. This filter is composed of two parts: one performs a moving-average (MA) of the incoming noise, the other makes an autoregression (AR) of the output signal onto itself. Hence the filter is expressed as a *linear* combination of the values of the noise and of the output itself at *previous* time steps, otherwise it would not be a causal linear one. The coefficients of the linear combination are chosen in order to minimize the variance of the input noise and from their values one can compute directly the power spectral density of former signal.

Parametric methods yield [29] a spectrum which is smoother and has a higher-frequency resolution than the one computed as a squared modulus of Fourier transform. At the same time, however, one needs to model the problem, i.e., one has to choose properly the number of terms to be used in the linear combination. Moreover the computational cost is higher for ARMA methods, but al-

ways suitable for real-time computation on a common workstation.

When applied to the time evolution of s with small values of Q, the ARMA analysis shows two peaks: one of them scales with Q according to the predictions of Nosé's model discussed in the previous section, while the other is independent on Q and corresponds to a frequency $\nu_A = 1.3 \pm 0.1$ THz. Figure 2 shows the results of ARMA analysis for three values of Q: 0.2, 0.1, and 0.05. The period of an atomic oscillation is approximately 10^{-13} s: one would therefore suspect that the nonscaling peak is due to the coupling between the bath s and the atomic coordinates: a frequency ν_A due to the atomic motion is introduced into the s dynamics.

For large values of Q the behavior is different: only one frequency band is observed, and it scales with Q. There is therefore a critical value Q_c at which the second frequency appears in the s spectrum.

Figure 3 shows a plot of the frequencies corresponding to the peaks in the ARMA analysis as a function of the Q values. Below $Q_c \approx 2$ the nonscaling peak appears. Both below and above Q_c there is a frequency ν_S which scales as predicted by Eq. (10), or $\nu_S \propto Q^{-1/\alpha}$ with an observed value $\alpha = 2.04 \pm 0.04$, in agreement with the expected value $\alpha = 2$. For the intercepts of the regression lines in the log-log plot we have two different values, as one can deduce from the different proportionality factors in Eqs. (10a) and (10b). Their ratio gives an estimate of $C_V = (3.1 \pm 0.1) N k_B$, which again is in agreement with the expected value ($3Nk_B$, Dulong and Petit law).

For $Q < Q_c$ the scaling frequency ν_S is higher than the "atomic" frequency ν_A and both ν_A and ν_S are present in the s spectrum. For $Q > Q_c$ instead one has $\nu_S < \nu_A$ and only ν_S shows up in for the s spectrum.

C. Power spectral density of the kinetic energy

It is interesting to compare the behavior of s with the corresponding kinetic energy (or instantaneous temperature) evolution. Figure 4(a) shows the kinetic-energy

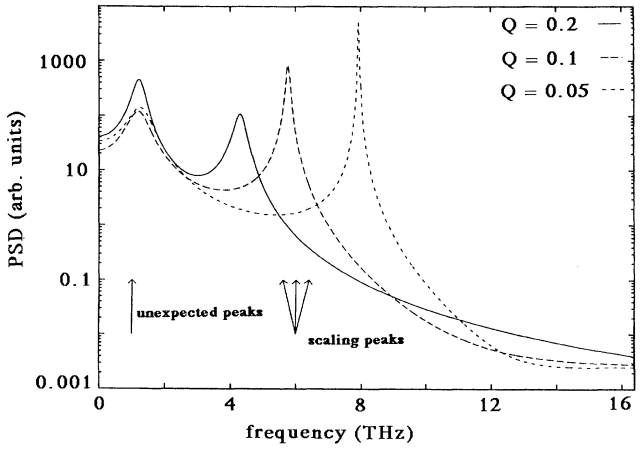

FIG. 2. ARMA analysis for the time evolution of s at three values of Q: $Q = 0.2$, $Q = 0.1$, and $Q = 0.05$.

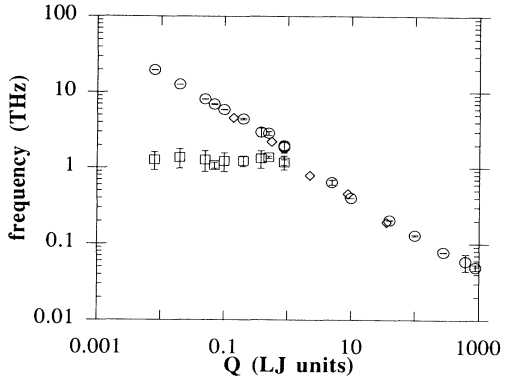

FIG. 3. Frequencies in the s spectrum (corresponding to the peaks in the ARMA analysis) as a function of Q. Circles indicate the frequencies scaling as predicted by relation (10). Squares are unexpected values and diamonds are from Nosé (Ref. [15]).

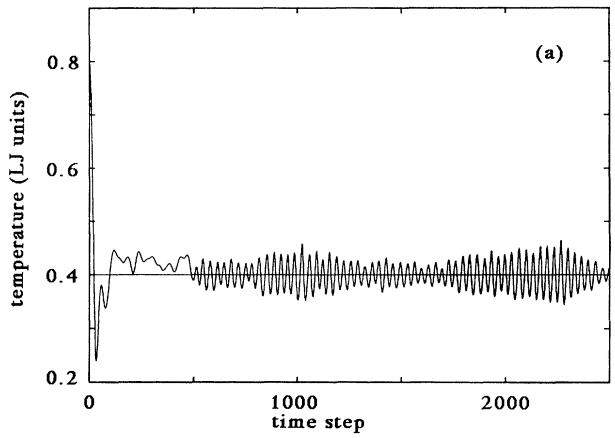

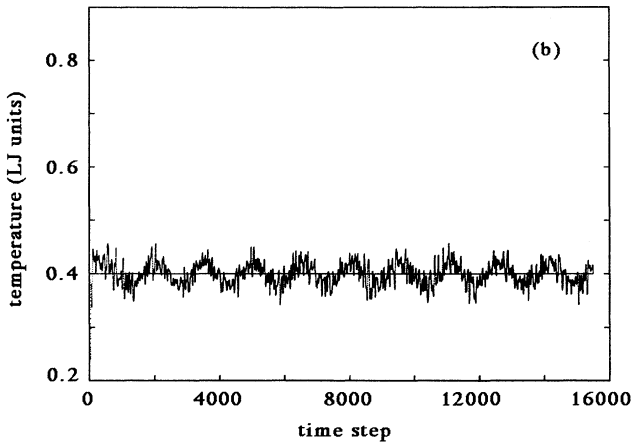

FIG. 4. Time evolution of the instantaneous temperature for $Q = 0.1$ (a) and $Q = 100$ (b). The initial 500 steps were performed at constant energy to equilibrate the system.

(KE) fluctuation for the case $Q=0.1$. The behavior of KE for $Q=100$ is shown in Fig. 4(b). By comparing with Fig. 1(a), one immediately notes that, for such large values of Q, the s oscillations are reflected in the KE behavior, producing a sinusoidal modulation. Additional, smaller scale (KE) fluctuations are clearly visible on top of such modulation. By comparison with Fig. 5, which shows the KE behavior for a constant-energy simulation, one infers that the additional fluctuations are due to the frequencies of the atomic motion. From these heuristic arguments one suspects that for these large values of Q the system should be characterized by (at least) two characteristic frequencies.

The ARMA analysis allows us to verify these arguments. In Fig. 6 we show the frequency spectrum of KE for three values of Q larger than Q_c. In this case, the peak at larger frequency does not scale, and instead there is a smaller frequency ν_S which scales according to Eq. (10). The plot of frequencies against Q, illustrated in Fig. 7, shows a nonscaling frequency ν_A corresponding to the atomic vibrations, and the scaling frequency ν_S which appears only for all values of Q.

The global picture is therefore the following: the extended system can be ideally partitioned into two sets: the set of the variables which describe the atoms, and the variable s which represents the heat bath. The atomic motion gives a frequency band centered around a characteristic frequency ν_A which corresponds to the inverse of the period of atomic oscillations. The s variable shows its own frequency ν_S which depends on the value of Q. When $Q>Q_c$ one has $\nu_S<\nu_A$. The time evolution of s is well approximated by a clean sinusoidal function, while the time evolution of KE looks like the sum of a sinusoidal function and a faster frequency with smaller amplitude. The spectrum of s shows only the ν_S peak and the KE spectrum exhibits both the ν_S and ν_A peaks: the perturbation of the heat bath on the atoms is shown as a (long wavelength) modulation in the kinetic energy, while the thermal vibrations do not influence s dynamics since they average out. In fact, one can derive from (7c) that

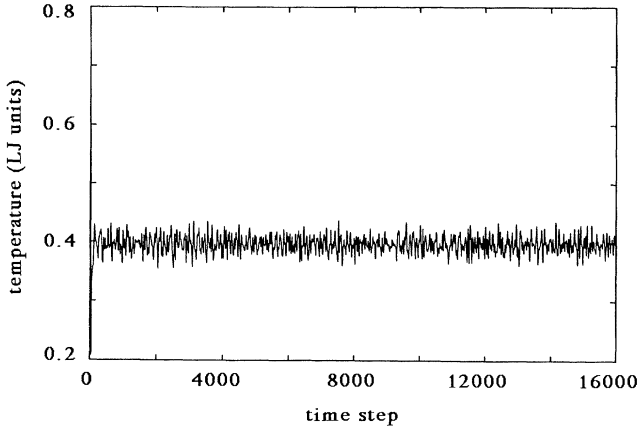

FIG. 5. Time evolution of the kinetic energy in a constant-energy simulation.

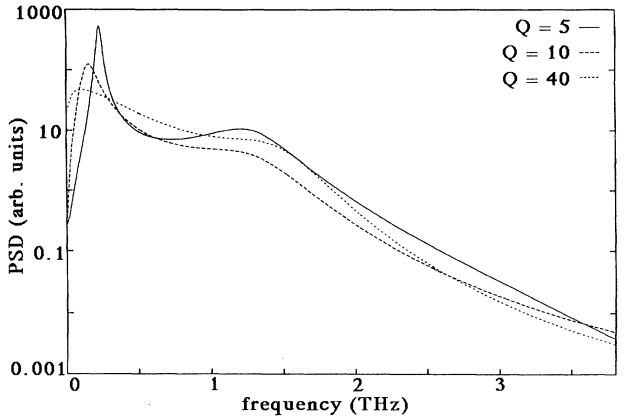

FIG. 6. Frequency spectrum of the kinetic energy for $Q=5$, $Q=10$, and $Q=40$.

$$\ln s \propto \int\int \left[K-\frac{g}{2}k_B T\right] dt\, dt' ,$$

where one can see that if the characteristic time for s is longer than the inverse of the frequency of kinetic energy K, such frequency cannot be transmitted to s.

In the opposite case ($Q<Q_c$) the relation $\nu_S>\nu_A$ holds. The spectrum of both s and KE shows ν_S and ν_A. The characteristic time for KE is longer than the one for s, and therefore ν_A survives to the integration. On the other hand, Eq. (7a) shows that the velocity of the particles is directly related to the value of s, and therefore and frequency in s is also present in KE, although for Q far from Q_c it can be (numerically) difficult to measure it.

When $Q\approx Q_c$ the "intrinsic" frequency ν_A is approximately equal to the "bath frequency" ν_S and the two peaks merge: both s and KE show a single peak in their frequency distributions.

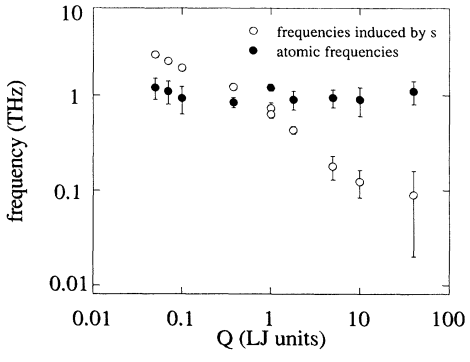

FIG. 7. Frequencies in the kinetic energy spectrum (corresponding to the peaks in the ARMA analysis) as a function of Q. Filled circles are atomic frequencies and empty circles are those induced by s.

D. Energy distribution and fluctuations

It is interesting to check whether the behavior discussed in the two last sections affects in any way the results of the simulation, i.e., if there is some consequence on the ability of the system to reproduce correctly a canonical ensemble. A way to assess it is to check for the energy distribution in the system.

We therefore computed the energy distribution at different Q values. It is well known that we can write the canonical partition function as the integral of an energy distribution

$$Z=\int_0^\infty \rho(E)dE \ .$$

We can expand ρ around the mean value of E, which turns out to be the mean value of H_0 in the simulation: hence we define

$$U=\langle H_0 \rangle$$

and the density ρ is a Gaussian of center U and width $\sigma=(k_B T_0^0 C_V)^{1/2}$,

$$Z=\int_0^\infty \frac{1}{N}\exp[-(U-E)^2/2\sigma^2]dE \ .$$

In Fig. 8(a) we plot the observed energy distribution after 85 ns of simulation (17 000 time steps) for $Q=0.008<Q_c$ (continuous line), along with the expected Gaussian distribution obtained by assuming $C_V=3NK_B$ (dashed line). The shape of the observed distribution is a Gaussian, but its width is too small: this means that energy fluctuations are underestimated and therefore the measure of the specific heat C_V is wrong. In the limiting case of $Q\to 0$ the system would be strictly isokinetic; i.e., at any time the kinetic energy of the system would equal its average value: the particle motion would be such that the velocity (averaged over all particles at any given time step) would be a constant.

Figure 8(b) shows the energy distribution for $Q\approx Q_c$: in this case the energy distribution is well fitted by the theoretically predicted Gaussian.

A case with $Q>Q_c$ ($Q=100$) is illustrated in Fig. 8(c). From the comparison between the expected distribution and the observed one it is clear that the energy distribution obtained from the simulation is completely wrong. The shape of the distribution is in fact quite different from a Gaussian, having a U-shaped form. To understand why this happens we need some arguments: let us consider a simulation in which $\langle s \rangle = 1+\varepsilon \approx 1$ (in most of our simulations $\langle s \rangle \approx 1.05$). In the Hamiltonian (2) we can therefore develop the term log(s):

$$H_N = H_0 + Q\dot{s}^2 + gk_B T\varepsilon$$

but along any trajectory H_N is conserved and each departure δE of the energy from its mean value $U=\langle H_0 \rangle$ is connected to the fluctuations $\delta s=\delta\varepsilon$ by

$$\delta H_N = 0 = \delta E + \delta K_s + gk_B T\delta S \ ,$$

where

$$\delta K_s = Q\delta(\dot{s}^2) \ .$$

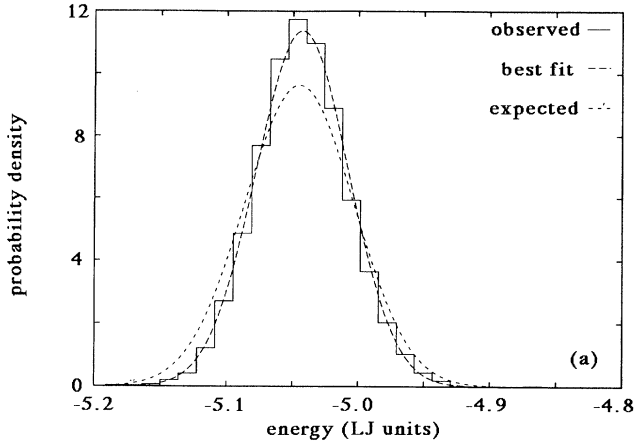

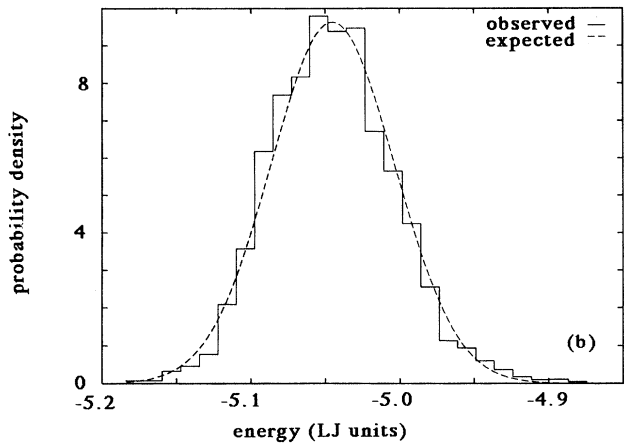

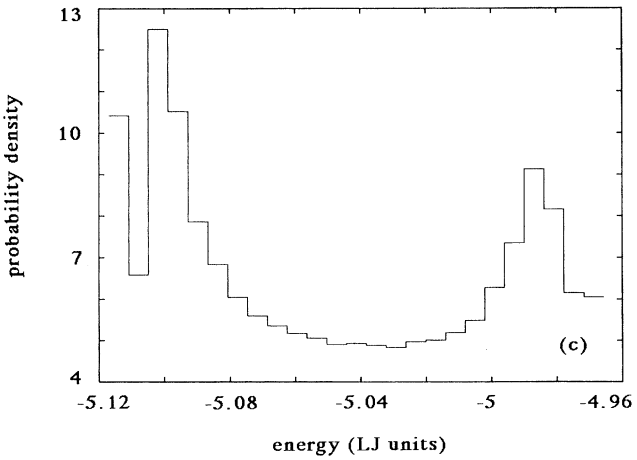

FIG. 8. Probability distribution of the total energy for $Q=0.08$ (a), $Q=0.5\approx Q_c$ (b), and $Q=100$ (c).

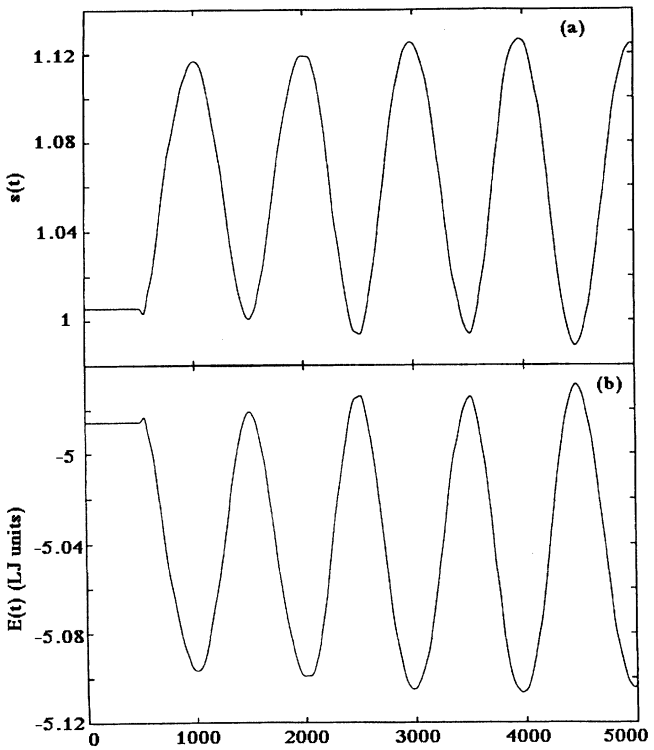

FIG. 9. Comparison between the time evolution of the variable s (a) and of the energy E (b). The initial 500 steps were performed at constant energy to equilibrate the system.

The term δK_s gives a negligible contribution to the total fluctuation because K_s is of order $\frac{1}{2}k_BT_0$ which is generally small in respect to the total value of the Hamiltonian $6N(\frac{1}{2}k_BT_0)$. Hence, at each time step we have the approximation relation

$$\delta E = -gk_BT_0\delta S \ .$$

This means that the graphs for $s(t)$ and $E(t)$ are equal and opposite (turned upside down, rescaled and shifted by proper factors), as shown in Fig. 9. As pointed before this graph is a (shifted) sine for large Q. Since in a sine most of the time is spent close to the maximum and minimum values, one expects a U-shaped distribution, as in fact we observe.

E. Convergence to the correct distributions

From what we have shown so far, one cannot rule out the possibility that for longer simulation times the correct energy distributions would be reproduced for both large and small Q values. In the case of Q small the Gaussian width could in fact grow with time. For large Q instead one could argue that the $K(t)$ graph is only approximately a sine, and that for large enough time it would lose coherence: the resulting energy distribution could then converge to the correct one. We investigated the time evolution of these distributions to check if this picture is in fact correct, and if so to estimate the time needed to obtain a correct measure.

TABLE I. Measure of the momenta $\mu_n = \langle (K - \langle K \rangle)^n \rangle$ where K is the kinetic energy, together with their ideal value. For a standard length run (85 ps) one observes that the estimate gets worse as Q decreases.

	μ_2	μ_3	μ_4	μ_5
expected	0.0306	0.0143	0.04	0.0308
$Q=0.07$	0.026	0.0117	0.035	0.026
$Q=0.05$	0.019	0.007	0.025	0.018
$Q=0.008$	0.0165	0.006	0.021	0.013

TABLE II. Values of the momenta μ_n for $Q < Q_c$ ($Q=0.07$) as a function of simulation length. The estimate seems not to converge to the expected values as simulation time grows.

($Q=0.07$)	μ_2	μ_3	μ_4	μ_5
expected	0.0306	0.0143	0.04	0.0308
$t=7.5$ ps	0.0168	0.0075	0.022	0.015
$t=25$ ps	0.0285	0.0127	0.036	0.026
$t=85$ ps	0.026	0.0117	0.035	0.026
$t=250$ ps	0.028	0.0123	0.036	0.026

An indication is given by higher momenta of the kinetic energy distribution. We followed the work by Cho and co-workers [24,25] and evaluated for small Q,

$$\mu_2 = \tfrac{3}{2}N(k_BT)^2 \ ,$$

$$\mu_3 = 3N(k_BT)^3 \ ,$$

$$\mu_4 = \tfrac{3}{2}N(\tfrac{9}{2}N+6)(k_BT)^4 \ ,$$

$$\mu_5 = 3N(15N+12)(k_BT)^5 \ ,$$

where $\mu_n = \langle (K - \langle K \rangle)^n \rangle$ and K is the kinetic energy. We report in Table I our measure of the momenta together with their ideal value. For a standard length run (85 ps) one observes that the estimate gets worse as Q decreases. In Table II we report the values of the momenta for a given Q (0.07) as a function of simulation length. The estimate seems not to converge to the expected values as simulation time grows. In fact, for $Q \to 0$ one expects an isokinetic dynamics, where all fluctuations are suppressed regardless of the length of the simulation. In Table III we show that instead for Q bigger but not too

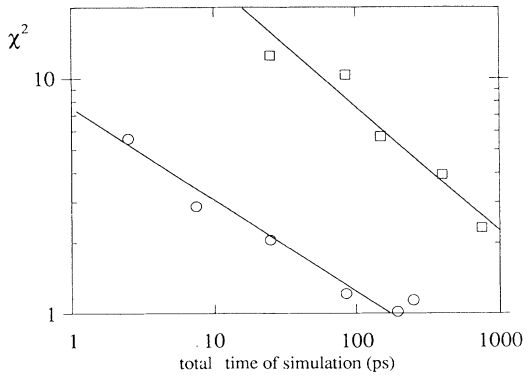

FIG. 10. Reduced χ^2 of the energy distribution as a function of the total simulation time for $Q=2.5$ (circles) and $Q=40$ (squares) for independent runs of simulation.

TABLE III. Values of the momenta μ_n for $Q > Q_c$ ($Q=2.5$). The estimate converges to the correct values.

($Q=2.5$) expected	μ_2 0.0306	μ_3 0.0143	μ_4 0.04	μ_5 0.0308
$t=2.5$ ps	0.028 (−8.5%)	0.023 (+38%)	0.0375 (−6.7%)	0.037 (+16%)
$t=7.5$ ps	0.0289 (−6%)	0.011 (−30%)	0.0384 (−4.2%)	0.024 (−28%)
$t=25$ ps	0.0333 (+8%)	0.0153 (+6.5%)	0.044 (+9.1%)	0.034 (+9%)
$t=85$ ps	0.0319 (+4%)	0.0147 (+2.7%)	0.042 (+4.8%)	0.032 (3.8%)
$t=250$ ps	0.0304 (−0.7%)	0.0138 (−3.6%)	0.040 (0%)	0.0306 (−0.7%)

far from Q_c ($Q=2.5$) the estimate converges to the correct values. For the case $Q > Q_c$, we also studied the χ^2 of the energy distribution. Figure 10 shows the reduced χ^2 values as a function of the total simulation time for independent runs. It is clearly seen that the estimate improves as a function of run length, and it is worse for larger values of Q. A fit of our data in a log-log plot gives a slope of -0.4 ± 0.1 for $Q=2.5$ and -0.50 ± 0.08 for $Q=40$, as expected if the estimate is statistically correct (i.e., χ^2 does decrease with the inverse square root of the total simulation time). On time scales suitable for the simulation we have correspondence between predictions and results only for $Q \approx Q_c$, while for $Q \gg Q_c$ we observe only a slow convergence to the right results. For $Q \ll Q_c$ we find that the fluctuations of the kinetic energy are underestimated and that this estimation does not improve even for longer simulations. We interpreted this fact showing that in the limit of $Q \to 0$ the Nosé-Hoover equations are equivalent to Gauss isokinetic dynamics. This result is in contrast with that of Cho and co-workers [24,25]. An attempt to explain the discrepancy of this results can be found in a recent work of Bylander and Kleinman [30].

F. Correlations

The mixing property requires that correlations between functions of dynamical variables vanish for large time lags. Hence we studied the autocorrelation of $s(t)$ for

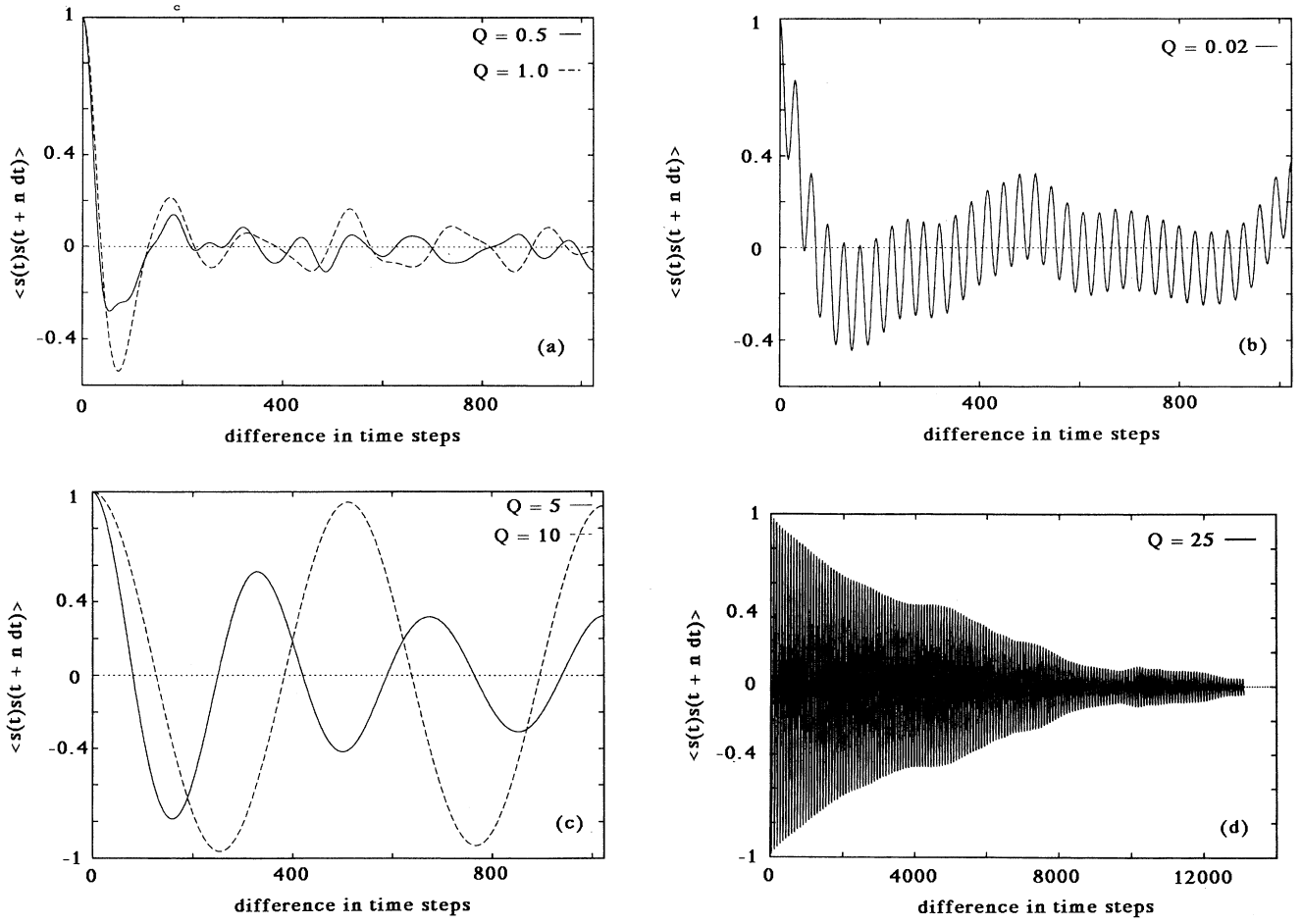

FIG. 11. Autocorrelation of $s(t)$: (a) $Q \approx Q_c$, (b) $Q \ll Q_c$, (c) $Q \gg Q_c$, (d) $Q \gg Q_c$ on a long-time scale ($Q=25$).

various values of Q. We find that in fact such correlation vanishes rapidly for Q near to Q_c, as can be seen in Fig. 11(a). For smaller and larger values of Q instead the system maintains memory [Figs. 11(b) and 11(c)]. For $Q \gg Q_c$ a damping of the oscillations on long time is clearly seen [Fig. 11(d)]. We therefore extensively studied the case of $Q \gg Q_c$ trying to find a characteristic decay time as a function of Q. We were, however, not able to find a law for predicting such time.

IV. CONCLUSIONS

In summary, we have investigated the behavior of a system defined by Nosé's Hamiltonian for a large range of values of the parameter Q which describes the coupling between the atoms and the thermal bath. Such systems are interesting because they can be used in the framework of classical mechanics to perform simulations at constant temperature. Moreover, Nosé's thermostat is used in the Car-Parrinello method to keep the electrons on the Born-Oppenheimer surface. Therefore it is important to know the limits of applicability of the method.

We examined the time evolution of the s variable and of the kinetic energy, and studied the frequencies involved. We observed a Q-independent frequency band due to the atomic oscillations, and a frequency which scales with Q and originates from the dynamics of the s variable. The two frequencies are at resonance at a critical value Q_c, which can be obtained by inverting the relation

$$\omega = \sqrt{2gk_B T_0 / Q_c} \ ,$$

where ω is the (average) characteristic frequency of the physical system (i.e., that of the atomic vibrations) and the expression on the right-hand side is Nosè's approximation for the Q dependence of ω at low Q.

We found that at Q_c, the dynamics samples the phase space so as to reproduce correctly, in a simulation of reasonable length, not only the average value of the kinetic energy but also its fluctuations, as expected from a canonical distribution. A simulation of comparable length at low values of Q tends to underestimate the fluctuations, while for large Q the energy distribution is completely wrong although the average value is correct. We investigated the dependence of the results on the simulation time, and found that in fact a better convergence can be observed for longer time in the case of large Q, while a longer simulation does not improve the results when Q is small.

In conclusion, the best choice is to perform a simulation with $Q \approx Q_c$. Q_c can be determined from the knowledge of a characteristic time of the system (typically the average time between atomic collisions).

ACKNOWLEDGMENTS

We thank S. Nosé, W. Hoover, A. Bulgac, D. Kusnezov, T. Cagin, K. Cho, and G. Ciccotti for interesting and useful discussions and for copies of unpublished work. This work has been supported in part by the Italian CNR "Progetto Finalizzato Sistemi Informatici e Calcolo Parallelo" (UO Reatto).

*Present address: ISAS-SISSA, Strada Costiera 11, 34100 Miramare Trieste, Italy.

[1] A. Rahman, Phys. Rev. **136**, A405 (1964).
[2] M. P. Allen and D. J. Tildesley, *Computer Simulation of Liquids* (Clarendon, Oxford, 1987); J. P. Hansen and I. R. McDonald, *Theory of Simple Liquids* (Academic, London, 1976); in *Molecular Dynamics Simulation of Statistical Mechanics Systems,* Proceedings of the International School of Physics "Enrico Fermi," Course XCVII, Varenna, 1985, edited by Wm. G. Hoover and G. Ciccotti (North-Holland, Amsterdam, 1986).
[3] Wm. G. Hoover, in *Molecular Dynamics,* Lecture Notes in Physics Vol. 258 (Springer-Verlag, Berlin, 1986).
[4] *Simulation Approach to Solids. Molecular Dynamics of Equilibrium Crystals and More,* edited by M. Ronchetti and G. Jacucci (Jaca Book–Kluwer, Dordrecht, 1990); *Simulation of Liquids and Solids, Molecular Dynamics and Monte Carlo Methods in Statistical Mechanics,* edited by G. Ciccotti *et al.* (North-Holland, Amsterdam, 1987).
[5] L. Verlet, Phys. Rev. **159**, 58 (1967).
[6] L. V. Woodcook, Chem. Phys. Lett. **10**, 257 (1971).
[7] Wm. G. Hoover, A. J. C. Ladd, and B. Moran, Phys. Rev. Lett. **48**, 1818 (1982); D. J. Evans, J. Chem. Phys. **78**, 3297 (1983).
[8] H. C. Andersen, J. Chem. Phys. **72**, 2384 (1980).
[9] S. Nosé, Molec. Phys. **52**, 255 (1984); J. Chem. Phys. **81**, 511 (1984).
[10] Wm. G. Hoover, Phys. Rev. A **31**, 1695 (1985).
[11] A consequence of the von Neumann–Birkhoff theorem, G. D. Birkhoff, Proc. Natl. Acad. Sci. (U.S.A.) **17** (1931); J. von Neumann, *ibid.* **18** (1932); see also Ref. [12].
[12] A. I. Kinchin, *Mathematical Foundations of Statistical Mechanics* (Dover, New York, 1949).
[13] A. I. Kinchin, *Mathematical Foundations of Statistical Mechanics* (Ref. [12]), p. 53.
[14] V. I. Arnold and A. Avez, *Problèmes Ergodiques de la Mèchanique Classique* (Gauthier-Villars, Paris, 1967).
[15] S. Nosé, Prog. Theor. Phys. Suppl. No. **103**, 1 (1991).
[16] J. Jellinek, J. Phys. Chem. **92**, 3163 (1988).
[17] J. Jellinek and R. S. Berry, Phys. Rev. A **38**, 3069 (1988).
[18] T. Cagin (unpublished).
[19] A. Bulgac and D. Kusnezov, Phys. Rev. A **42**, 5045 (1990).
[20] D. Kusnezov, A. Bulgac, and W. Bauer, Ann. Phys. (N.Y.) **204**, 155 (1990).
[21] D. Kusnezov and A. Bulgac, Michigan State University Report No. MSUCL-788, 1991 (unpublished).
[22] H. A. Posch, Wm. G. Hoover, and F.J. Vesely, Phys. Rev. A **33**, 4253 (1986); and Ref. [16].
[23] S. Nosé, Phys. Rev. E **47**, 164 (1993).
[24] K. Cho and J. D. Joannopoulos, Phys. Rev. A **45**, 7089

(1992).
[25] K. Cho, J. D. Joannopoulos, and L. Kleinmann, Phys. Rev. E **47**, 3145 (1993).
[26] S. Nosé, in *Computer Simulation in Material Sciences,* Vol. 205 of NATO ASI, Series E: Applied Sciences, edited by M. Meyer and V. Pontikis (Plenum, New York, 1991); see also Ref. [7].
[27] G. J. Martyna, M. L. Klein, and M. Tuckerman, J. Chem. Phys. **97**, 2635 (1992).
[28] Sir L. Marple, Jr., *Digital Spectral Analysis with Applications* (Prentice-Hall, Englewood Cliffs, NJ, 1987), S. M. Kay, *Modern Spectral Estimations Theory and Applications* (Prentice-Hall, Englewood Cliffs, NJ, 1988).
[29] S. Cerutti, R. Balzarotti, G. Baselli, and D. Liberati, Biomed. Meas. Infor. Contr. **1**, 111 (1986); G. Ingrassia and F. D. Di Tolla, Istituto per la Ricerca Scientifica e Tecnologica, internal report, Trento, Italy, 1989 (unpublished), and (private communication).
[30] D. M. Bylander and L. Kleinman, Phys. Rev. B **46**, 13 756 (1992).